On the Wafer/Pad Friction of Chemical–Mechanical Planarization (CMP) Processes—Part II: Experiments and Applications

Jingang Yi, *Member, IEEE*

***Abstract*—This paper presents the experimental validation and some application examples of the proposed wafer/pad friction models for linear chemical–mechanical planarization (CMP) processes in the companion paper. An experimental setup of a linear CMP polisher is first presented and some polishing processes are then designed for validation of the wafer/pad friction modeling and analysis. The friction torques of both the polisher spindle and roller systems are used to monitor variations of the friction coefficient *in situ*. Verification of the friction model under various process parameters is presented. Effects of pad conditioning and the wafer film topography on wafer/pad friction are experimentally demonstrated. Finally, several application examples are presented showing the use of the roller motor current measurement for real-time process monitoring and control.**

***Index Terms*—Chemical–mechanical planarization (CMP), friction, process modeling and monitoring, shallow trench isolation (STI).**

I. Introduction

THE FRICTION characteristics between the wafer and the polishing pad in chemical–mechanical planarization (CMP) processes play an important role in the process performance. Sikder *et al.* [2] discussed measuring the coefficient of friction (COF) under various polishing parameters, such as table rotating speed and polishing downforce. A prototype of a rotary CMP polisher and blanket oxide wafers were used in Sikder *et al.* [2] without pad conditioning. In Homma *et al.* [3], a linear relationship between the CMP material removal rate and the wafer/pad friction force has been demonstrated experimentally. However, no analytical relationship between the wafer/pad friction characteristics and the polishing parameters was investigated in Sikder *et al.* [2] or Homma *et al.* [3]. In the first part of this study [1], a friction modeling and estimation scheme was proposed for both blanket oxide and patterned wafers. The friction model proposed by Yi [1] is based on a distributed LuGre dynamic friction model for a linear CMP polisher and the proposed methods can be extended and applied to rotary CMP polishers. A quantitative relationship between the spindle and roller friction torques and the polisher parameters, such as wafer carrier speed, polishing pad speed, and wafer carrier downforce was derived. Effects of pad conditioning and the patterned wafer topography on friction modeling were also investigated in [1]. In this paper, we discuss the experimental validation of the wafer/pad friction model and analysis in [1]. The spindle and roller motor current measurements are used to monitor *in situ* the friction variations during a polishing process. Friction model parameters are first estimated and the model is then used to predict the friction characteristic.

Manuscript received May 27, 2004; revised March 4, 2005.

The author was with Lam Research Corporation, Fremont, CA 94538 USA. He is now with the Department of Mechanical Engineering, Texas A&M University, College Station, TX 77843 USA (e-mail: jgyi@tamu.edu.).

Digital Object Identifier 10.1109/TSM.2005.852100

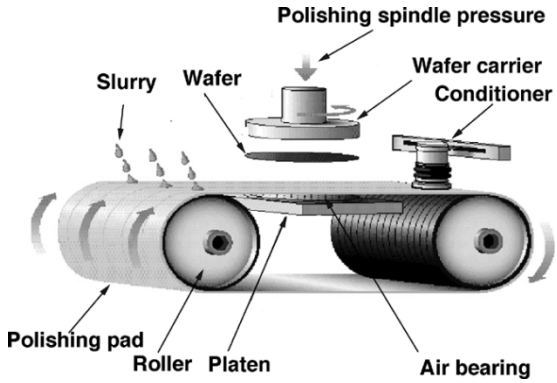

Fig. 1. Schematic of the Lam linear CMP systems.

This paper is organized as follows. Section II reviews the main results of the wafer/pad friction model in [1] for a linear CMP polisher. In Section III, a relationship between the motor current measurement and the friction and polishing process parameters is presented. The experimental design used for this study is also discussed. In Section IV, estimations of the friction model parameters and mechanical system parameters are first discussed. Experimental validations of the friction model are then presented. Discussions of the dependency of various process parameters on the friction model are also included in this section. Several application examples of friction monitoring are illustrated in Section V. Concluding remarks and future development are presented in Section VI.

II. Wafer/Pad Friction Model

This study focuses on linear CMP processes. Fig. 1 shows a schematic of the linear planarization technology (LPT) provided by Lam Research Corporation. With the LPT design, a polishing pad moves at an adjustable speed and a wafer is held by a wafer carrier against the polishing pad. The spindle assembly holding the wafer carrier provides the controllable downforce pressure against the pad. Beneath the polishing pad, an air-bearing platen with independently controlled concentric rings of air-pressure channels pushes the polishing pad against the wafer surface.

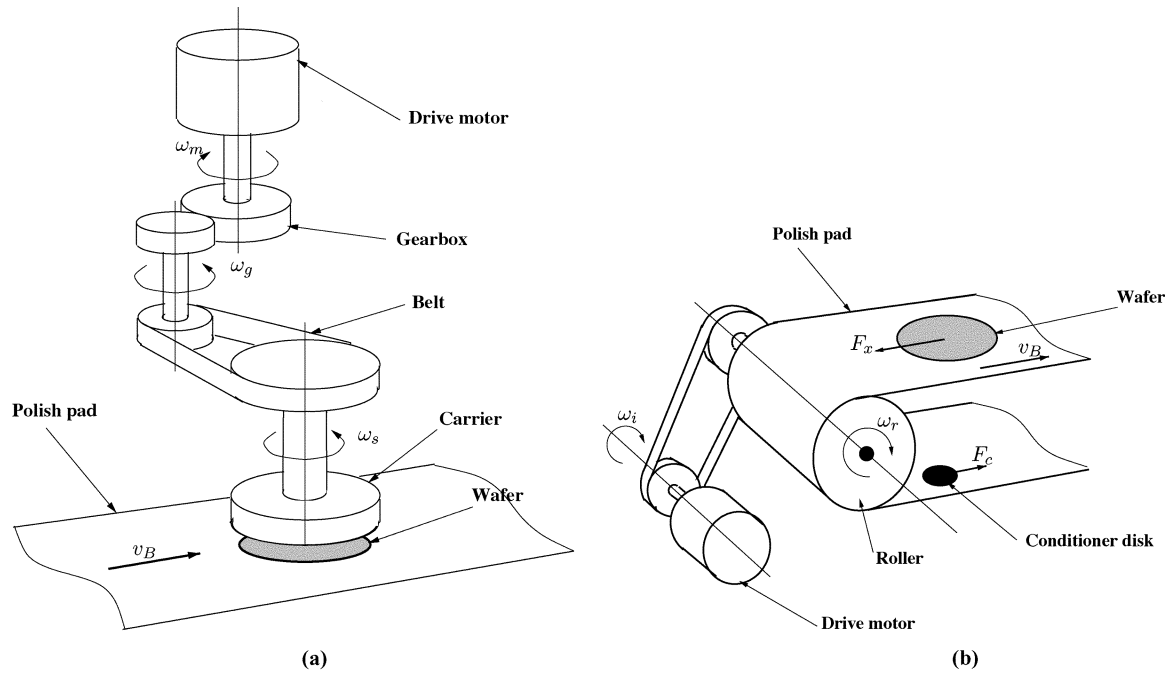

Fig. 2. Kinematic diagram of the polishing set. (a) Spindle system. (b) Roller system.

Each of the pressure channels is adjusted to conform the pad to the wafer surface and therefore achieve the planarization.

In [1], an analytical model was proposed to estimate the torques applied by the spindle and roller motors due to the wafer/pad contact friction. The spindle torque $M^{\mathrm{s}}_{\mathrm{patt}}$ and roller torque $M^{\mathrm{r}}_{\mathrm{patt}}$ for a patterned wafer (e.g., shallow trench isolation (STI) devices) can be estimated as

$$M^{\mathrm{s}}_{\mathrm{patt}}(t) = \gamma_{\mathrm{patt}}(t)\left[1+\gamma_\mu \gamma^{\mathrm{s}}_{\mathrm{cond}}(t)\right] M^{\mathrm{s}} \quad (1)$$

$$M^{\mathrm{r}}_{\mathrm{patt}}(t) = \gamma_{\mathrm{patt}}(t)\left[1+\gamma_\mu \gamma^{\mathrm{r}}_{\mathrm{cond}}(t)\right] M^{\mathrm{r}} \quad (2)$$

where M^{s} and M^{r} are the spindle and roller friction torques that arise when polishing blanket wafers without pad conditioning. γ_{patt} is the pattern effect factor, γ_μ is the friction coefficient amplification factor, and $\gamma^{\mathrm{r}}_{\mathrm{cond}}$ and $\gamma^{\mathrm{s}}_{\mathrm{cond}}$ are, respectively, the pad conditioning factors of the spindle and roller systems.

For a CMP process with a high polishing pad speed and a slow wafer carrier rotating speed, we can obtain the spindle and roller friction torques as

$$M^{\mathrm{s}} = \frac{1}{4} p_0 \pi R^4 \omega \left(\frac{\mu_s}{\theta v_B} + 2\sigma\right) \quad (3)$$

$$M^{\mathrm{r}} = p_0 \pi R^2 R_r \left(\frac{\mu_s}{\theta} + \sigma v_B\right) \quad (4)$$

where p_0 is the applied external polishing pressure, R is the wafer radius, v_B is the polishing pad speed, ω is the wafer carrier rotating speed, and μ_s/θ and σ are wafer/pad friction model parameters, respectively [1].

Pad conditioning factors $\gamma^{\mathrm{r}}_{\mathrm{cond}}$ (spindle) and $\gamma^{\mathrm{s}}_{\mathrm{cond}}$ (roller) are determined by the settings of the pad conditioner systems such as the conditioner downforce and sweep frequency, etc. γ_μ is determined by the contact characteristics of the polishing pad and conditioner disk [4]. For patterned wafer polishing, γ_{patt} captures the effects of pattern density ρ and device feature length (e.g., pitch width for STI devices) on the friction torques. For more details on the friction modeling and analysis, readers can refer to [1].

III. Experimental Setup

The friction model (1) and (2) provides a means to calculate the magnitude of the friction moments during a CMP process. However, we need to know the friction model parameters such as σ and θ etc. In order to identify the friction model parameters, in this section, we discuss the use of measurements of the spindle and roller motor currents to estimate these parameters. The hardware setup of the CMP polisher system is first introduced and a set of CMP processes are then designed.

A. System Setup

Fig. 2 shows a schematic of the spindle and roller systems. For the spindle system, a direct current (dc) motor is used to drive the spindle rotation. A gearbox and belt transmission system transfers the rotating motion and converts the fast motor speed into a slower and more accurate spindle rotation. The spindle speed is regulated by a proportional-integral-derivative (PID) controller to the target wafer carrier speed set up by the users. For the roller system, an alternating current motor is used to control the roller speed at a given value by a pulsewidth modulation (PWM) servo controller. Both the spindle and roller motor currents can be monitored without adding any new hardware components.

Consider the spindle system dynamics [see Fig. 2(a)]. Denote T^{s}_m to be the output torque of the spindle dc motor, T^{s}_i the torque transmitted to the spindle system (wafer carrier), T^{s}_o the load torque applied on the motor axis, T^{s}_{fm} and T^{s}_{fs} the friction torques from the mechanical components on the motor and spindle systems, respectively. Let ω_m, ω_g, and ω be the angular

speeds of the motor, gearbox and spindle systems, respectively. For the motor subsystem, we can obtain the dynamics as

$$T_m^{\rm s} - T_{fm}^{\rm s} - T_o^{\rm s} = J_m \dot{\omega}_m \tag{5}$$

where J_m is the mass inertia of the motor axis. Similarly, for the spindle system, we can obtain

$$T_i^{\rm s} - T_{fs}^{\rm s} - T_w^{\rm s} = J_s \dot{\omega} \tag{6}$$

where $T_w^{\rm s}$ is the magnitude of the spindle friction moment, i.e., $T_w^{\rm s} = M^{\rm s}$, and J_s is the mass inertia of the spindle system. Assuming no energy loss for the gearbox and belt transmission, we obtain

$$T_i^{\rm s} \omega_m = T_o^{\rm s} \omega. \tag{7}$$

Denote the gearbox and belt transmission ratios as r_g and r_b, respectively. We can obtain

$$\omega_m = r_g \omega_g = r_g r_b \omega = K_r^{\rm s} \omega \tag{8}$$

where $K_r^{\rm s} = r_g r_b$ is the combined gearbox and belt transmission ratio. Using (5)–(8), we obtain

$$T_m^{\rm s} - T_{fm} - \frac{T_{fs}^{\rm s}}{K_r^{\rm s}} - \frac{T_w^{\rm s}}{K_r^{\rm s}} = \left(\frac{J_s}{K_r^{\rm s}} + K_r^{\rm s} J_m \right) \dot{\omega}. \tag{9}$$

Before the wafer carrier touches down on the polishing pad, the spindle starts rotating at speed ω and then pushes the wafer carrier down against the pad. We can consider the steady-state rotation $(\dot{\omega} = 0)$ before and after the spindle touchdown. Before the spindle system touches down, we have $T_w^{\rm s} = 0$ and using $\dot{\omega} = 0$, (9) becomes

$$T_{m0}^{\rm s} = T_{fm}^{\rm s} + \frac{T_{fs}^{\rm s}}{K_r^{\rm s}} \tag{10}$$

where $T_{m0}^{\rm s}$ is the motor torque that overcomes the mechanical friction moments. Once the spindle touches down, similarly we have

$$T_{m1}^{\rm s} = T_{fm}^{\rm s} + \frac{T_{fs}^{\rm s}}{K_r^{\rm s}} + \frac{T_w^{\rm s}}{K_r^{\rm s}} \tag{11}$$

where $T_{m1}^{\rm s}$ is the motor torque that overcomes both the wafer/pad friction moment and the mechanical friction moments. Since the mechanical friction moments do not change before and after the spindle touchdown, from (10) and (11), we obtain

$$T_w^{\rm s} = M^{\rm s} = K_r^{\rm s} \left(T_{m1}^{\rm s} - T_{m0}^{\rm s} \right) = K_r^{\rm s} K_i^{\rm s} \left(I_{m1}^{\rm s} - I_{m0}^{\rm s} \right). \tag{12}$$

The dc motor electromechanical relationship $T = K_i^{\rm s} I$ is used in the above equation, where $K_i^{\rm s}$ is the torque/current constant for the dc motor and $I_{m1}^{\rm s}$ and $I_{m0}^{\rm s}$ are the motor currents before and after the spindle touches on the pad.

From (12) we know that by measuring the spindle motor currents, we can estimate the wafer/pad friction torque during the polishing process. Combining (12) and (3), we can estimate the friction model parameters such as μ_s and σ.

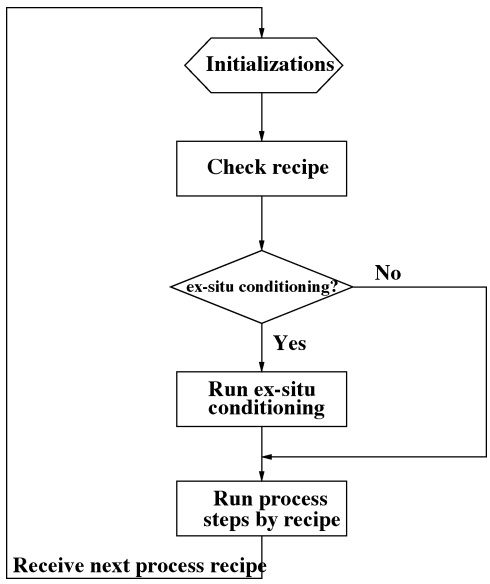

Fig. 3. Flow chart of process sequences on one polishing module.

TABLE I
SOME CONSTANTS FOR THE SPINDLE SYSTEM

Spindle system constants	$K_i^{\rm s}$	r_g	r_b
Values	0.3341 Nm/A	15	2

Following a similar derivation, we can obtain the torque-current relationship for the roller system.

$$T_w^{\rm r} = M^{\rm r} = K_r^{\rm r} K_i^{\rm r} \left(I_{m1}^{\rm r} - I_{m0}^{\rm r} \right) \tag{13}$$

where $K_r^{\rm r}$ is the ratio of the roller speed and roller motor speed, $K_i^{\rm r}$ is the motor torque/current constant, and $I_{m0}^{\rm r}$ and $I_{m1}^{\rm r}$ are the roller motor currents under idle and polishing states, respectively.

B. Process Description

Each CMP process is running under a set of user-defined process sequences, called recipes. A recipe includes a set of complex process and polisher system configurations. The cluster tool computer (CTC) system loads the recipes and then executes the process sequences. Fig. 3 shows a flow of a typical process sequence on one polishing module. Normally the system checks the recipe first to make sure the recipe setting is correct and feasible under the current system configuration. If the recipe setting is correct, then the system makes preparations for the process such as pumping the slurry into the system and indexing the wafer carriers etc. The polishing process starts with the *ex situ* pad conditioning recipe and then the process recipe. *Ex situ* pad conditioning is executed before the wafer carrier touches down on the pad and *ex situ* pad conditioning can be set independently with *in situ* pad conditioning and the polishing recipes. This is important for wafer/pad friction

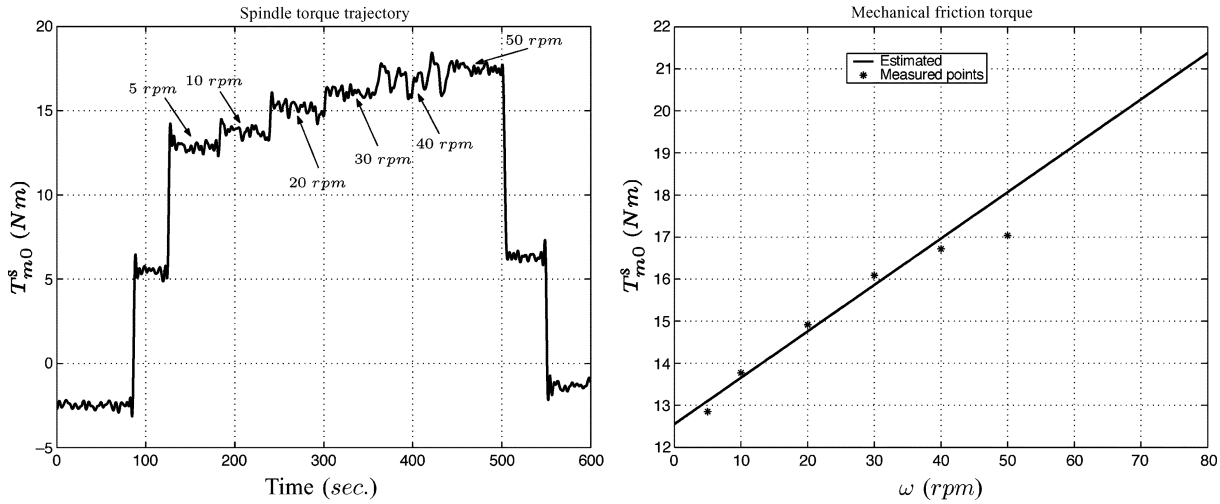

Fig. 4. Estimation of mechanical friction torque for the spindle system. (a) Measured torque at various wafer carrier speeds. (b) Estimated friction torque.

TABLE II
PROCESS PARAMETERS OF CMP PROCESSES

Slurry flowrate	Head pressure	Air-bearing pressures/Platen height	Head speed
150 ml/min	5 psi	5 psi/13psi/45psi/11psi/0/0/ 9 mil	20 rpm

coefficient estimation since pad conditioning has a significant impact on the wafer/pad friction characteristic.

IV. FRICTION MODEL IDENTIFICATION AND VALIDATION

A. Parameter Identification

In order to use the proposed friction model, we have to obtain the information of the mechanical friction torques of the spindle and roller systems (i.e., $I^{\rm s}_{m0}$ and $I^{\rm r}_{m0}$) and the model parameters, such as μ_s/θ and σ, etc.

The friction torque among moving mechanical components can be modeled as having two parts: Coulomb and linear viscous friction torques. For the spindle system, (10) can be rewritten as

$$T^{\rm s}_{m0} = f_v\omega + f_c \tag{14}$$

where f_c and f_v are the Coulomb and viscous friction coefficients, respectively. Therefore, (14) can be used to estimate $T^{\rm s}_{m0}$ by measuring the mechanical friction torque at various spindle speeds. Table I lists the spindle motor constants and the mechanical transmission ratios of the spindle system. Fig. 4(a) shows an experiment that we ran on a Lam Teres CMP polisher with various spindle speeds. Note that the mechanical friction torque is more stable at a low wafer carrier rotating speed than that at a high speed. A least-square (LS) estimation of friction coefficients is

$$\hat{f}_v = 0.1103\,\mathrm{Nm}\cdot\mathrm{s}, \quad \hat{f}_c = 12.5533\,\mathrm{Nm}. \tag{15}$$

Fig. 4(b) shows the estimated mechanical friction torque and experimental measurements. It can clearly see that the estimation given by (14) predicts the mechanical friction torque accurately for the operating range of spindle speed.

With the estimation of $T^{\rm s}_{m0}$, the spindle moment $M^{\rm s}$ can be calculated and is then used to estimate the model parameters μ_s/θ and σ. Equation (3) can be rewritten into the following form:

$$M^{\rm s} = p_0E_1(v_B,\omega)\left(\frac{\mu_s}{\theta}\right) + \left(\frac{1}{2}\pi p_0\omega R^4\right)\sigma = \mathbf{X}^T\Theta \tag{16}$$

where

$$\mathbf{X}^T = \left[p_0E_1(v_B,\omega)\ \frac{1}{2}\pi p_0\omega R^4\right], \quad \Theta = \left[\frac{\mu_s}{\theta}\ \sigma\right]^T.$$

An LS estimation of the model parameters $\hat{\Theta}$ can be obtained as

$$\hat{\Theta} = (\mathbf{X}\mathbf{X}^T)^{-1}M^{\rm s}.$$

To obtain a fairly large spindle torque, by (3), a set of polishing processes with pad speed variations at a relatively low-speed range are designed. The CMP process parameters used in the experiments are listed in Table II. No pad conditioning is used in the experiments. Fig. 5(a) shows the measured spindle torque at various pad speeds and the mechanical friction torque at a wafer carrier rotating speed $\omega = 20\ \mathrm{r/min}$.

From the measured spindle torque $M^{\rm s}$ at $v_B = 50$, 75, 100, and 125 ft/min, an estimation of model parameters can be obtained

$$\hat{\Theta} = [0.323 \quad -0.085]^T.$$

Note that steady-state spindle torques are used for the parameter estimation since the friction coefficient μ_s is decaying during the CMP processes without pad conditioning. Fig. 5(b) shows the estimated and measured spindle torques as a function of

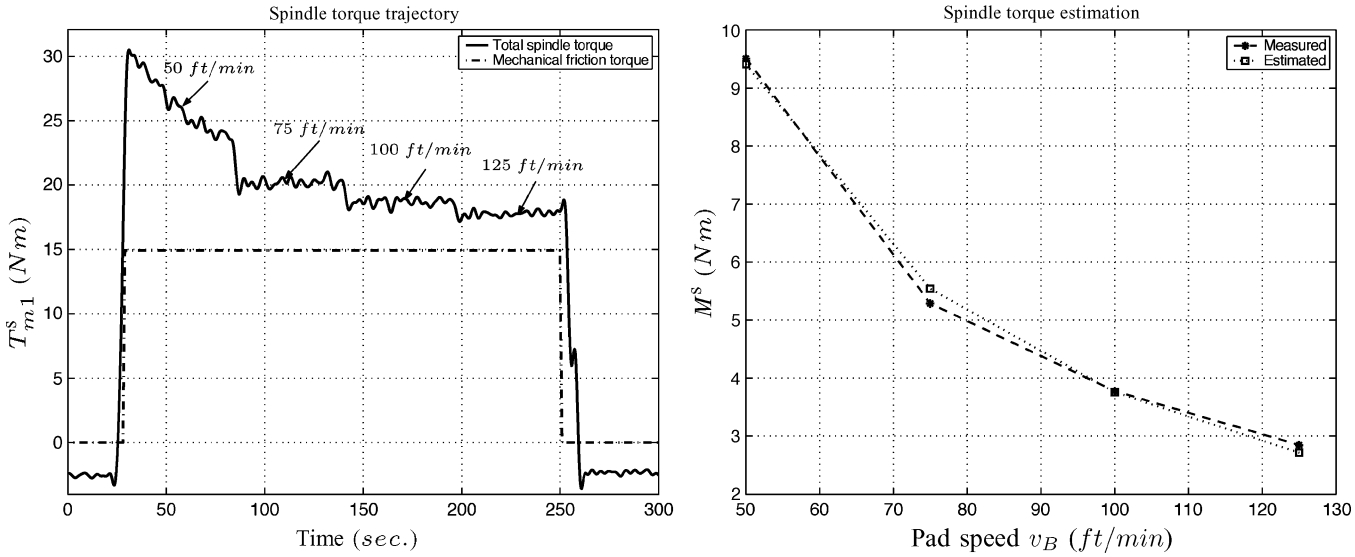

Fig. 5. Estimation of friction model parameters using the spindle system. (a) Measured torque at various pad speeds. (b) Estimated spindle torques.

TABLE III
EX SITU PAD CONDITIONING PARAMETERS OF THE TESTING PROCESSES

Slurry flowrate	Pad speed	Conditioner downforce	Number of sweeps	Sweep time
150 ml/min	150 ft/min	7 lbf	4	7 $sec.$

pad speed v_B. The estimated spindle torque matches the measurements very well. In the following sections, these estimated parameters are used to compute the spindle and roller system torques.

B. Model Validation

In this section, we present a set of comprehensive experiments to validate the friction models proposed in [1]. A baseline CMP process is used to study the pad conditioning effect. Some other processes are compared with the baseline process by only changing one process parameter at a time. The baseline process setting is listed in Table II with a pad speed $v_B = 250$ ft/min and *ex situ* pad conditioning is used with a list of settings in Table III. 200-mm thermal oxide blanket wafers, Cabot SS12 slurry and a Rodel IC 1000 pad are used on a Lam Teres CMP polisher.

1) Pad Conditioning Effects: Fig. 6 shows the wafer carrier external pressure p_0, pad speed v_B, spindle motor torque $M^{\rm s}$ and roller motor current measurements $M^{\rm r}$[1] for a baseline process without pad conditioning. The polishing process time is 168 s. From Fig. 6(a), we can see a small periodic oscillation with an approximate period equal to that of the wafer carrier rotation ($T = 3$ s for 20 r/min). This is due to the gimballing mechanism design of the polishing wafer carrier and the fact that the axis of the spindle system is not perfectly perpendicular to the polishing pad surface. It can clearly see that the friction coefficient μ_s is decaying without pad conditioning [Fig. 6(d)]. This has been observed and reported by some other researchers [2]. The spindle torque during the polishing process is larger than the mechanical friction torque by only a small amount [Fig. 6(c)]. Namely, the spindle torque that overcomes the wafer/pad friction $M^{\rm s}$ is relatively small. This is consistent with (3) under the case of a high pad speed v_B. For this reason, it is not accurate to use the spindle torque information to estimate the decay of the wafer/pad friction coefficient. Fortunately, we find that the roller torque instead has a significant change during the polishing process [Fig. 6(d)].

A curve-fitting algorithm is used to estimate the decay of friction coefficient μ_s between wafer and pad during the polishing process. The same curve is then used to predict the spindle torque [dot-line curve shown in Fig. 6(c)]. The estimated spindle curve fits very well with measured spindle torque (solid-line curve in the same figure). This is because the ratio of spindle and roller torques is approximately constant at a high pad speed. This observation can be calculated by (3) and (4) and from the fact that σ is much smaller than microseconds, we obtain

$$\frac{M^{\rm s}}{M^{\rm r}} = \frac{\omega R^2\left(\frac{\mu_s}{\theta v_B} + 2\sigma\right)}{4R_r\left(\frac{\mu_s}{\theta} + \sigma v_B\right)} \approx \frac{\omega R^2}{4R_r v_B}$$

which is a constant for a fixed pad speed v_B and a fixed wafer carrier speed ω.

The pad conditioning effect can be seen from the spindle and roller motor torques. Fig. 7 shows the spindle and roller motor torques using the same baseline process recipe and a 100%[2] pad conditioning with conditioner disk sweep time $T_c = 7$ s and conditioner downforce $F_c = 7$ lbf.

From Fig. 7(a), we find that the spindle torque just overcomes the mechanical friction torque. The oscillation period for the

[1]The motor current reading (in voltage) provided by the motor circuits is used as the indicator of the roller motor torque in this paper.

[2]The percentage of conditioning is defined as the ratio of the total conditioning process time over the entire process time.

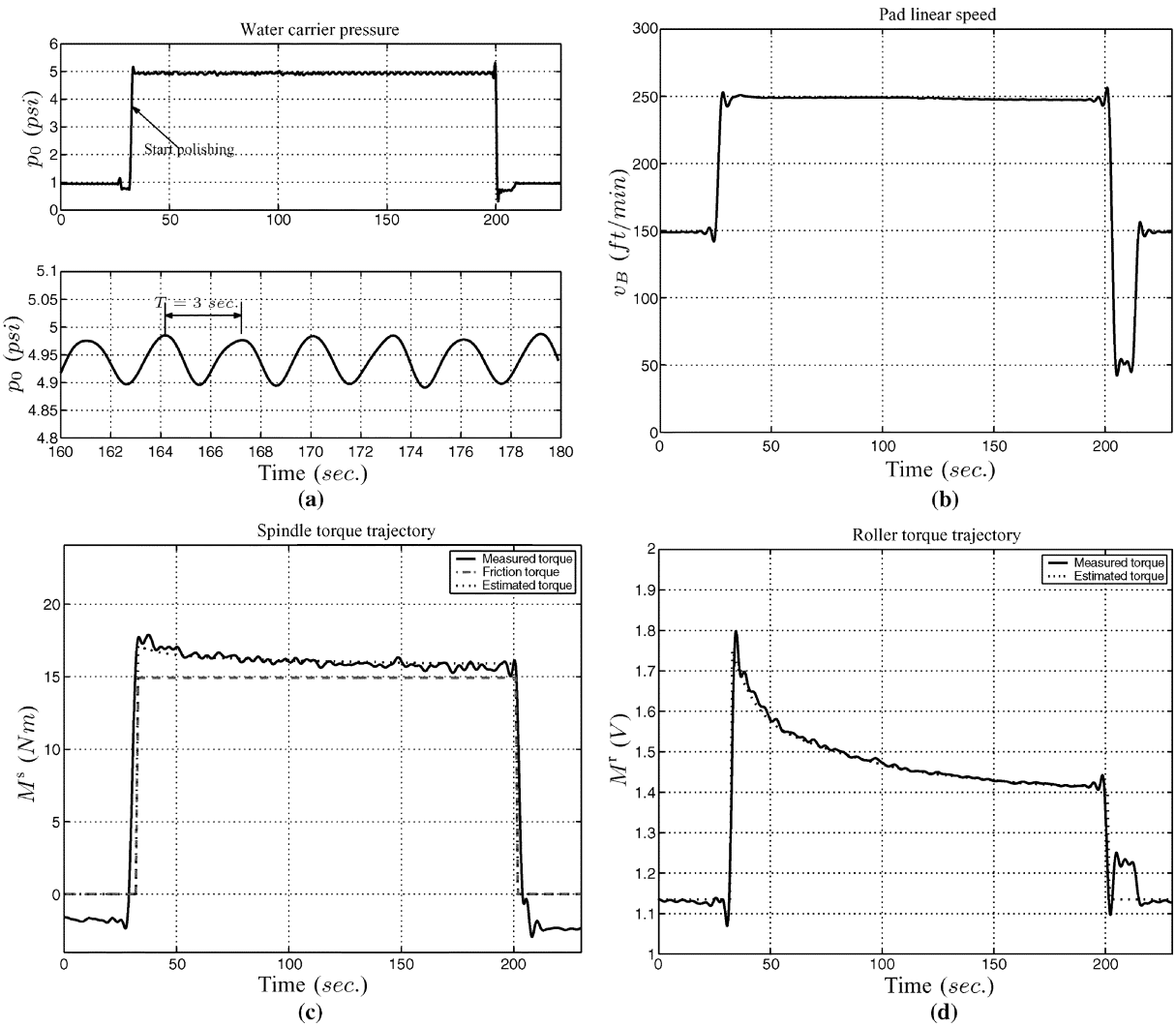

Fig. 6. Example of a baseline process without pad conditioning. (a) Wafer carrier pressure. (b) Pad speed. (c) Spindle motor torque. (d) Roller motor current.

measured spindle torque is around 15 s, which is very close to the two-sweep pad conditioning time set in the recipe (14 s). The estimations of both spindle and roller torques are very close to the measured values. In the estimation, $\gamma_\mu = 0.8$, $\beta_1 = 0.7$, and $\beta_2 = 0.3$ are used. The estimated torques fit the measurements very well. Compared with Fig. 6, another important observation in Fig. 7 is that under pad conditioning both spindle and roller motor torques are maintained at constant levels instead of decaying as they do without pad conditioning (Fig. 6).

Figs. 8 and 9 show the measured and estimated spindle and roller motor torques for a baseline process with 50% 7 lbf and 100% 3 lbf pad conditioning, respectively. It can clearly see that the proposed models give accurate estimations of both spindle and roller motor torques.

Combining all the pad conditioner tests, Fig. 10 compares spindle and roller torques under various process settings. The impact of pad conditioning on the motor torques is clearly demonstrated. Fig. 10(b) shows that the roller torque is much more sensitive to the process parameters and the pad conditioning variations. With pad conditioning, the motor torques are maintained at a constant level. Without pad conditioning, on the other hand, the motor torques keep dropping. Conditioner downforce also plays an important role for the motor torques. The roller motor torque with 3 lbf conditioner downforce is much smaller than that with 7 lbf downforce. The higher conditioner downforce increases the polishing pad roughness level and, therefore, yields a higher friction coefficient factor γ_μ.

2) Pad Speed Variations: In order to understand how the polishing pad speed affects the wafer/pad friction, a four-step process is run. Pad conditioning is not used in the process. The same baseline recipe as for the previous tests is used. Pad speed is varying from 100 to 400 ft/min with an 100 ft/min increase for each step. Each process step lasts 30 s. Fig. 11 shows the spindle and roller motor torques, pad speed, and wafer carrier external pressure.

Fig. 11(a) illustrates how the spindle torque changes with the pad speed increasing from 100 to 400 ft/min. When the pad speed changes from 100 to 200 ft/min, it can clearly see that the spindle torque decreases about 5 Nm. However, we cannot distinguish the spindle torque change for steps afterward. This observation verifies the friction model in [1]: spindle torque is relatively small even though it is proportional to the reciprocal of the pad speed [(3)]. Another interesting fact is that at the high

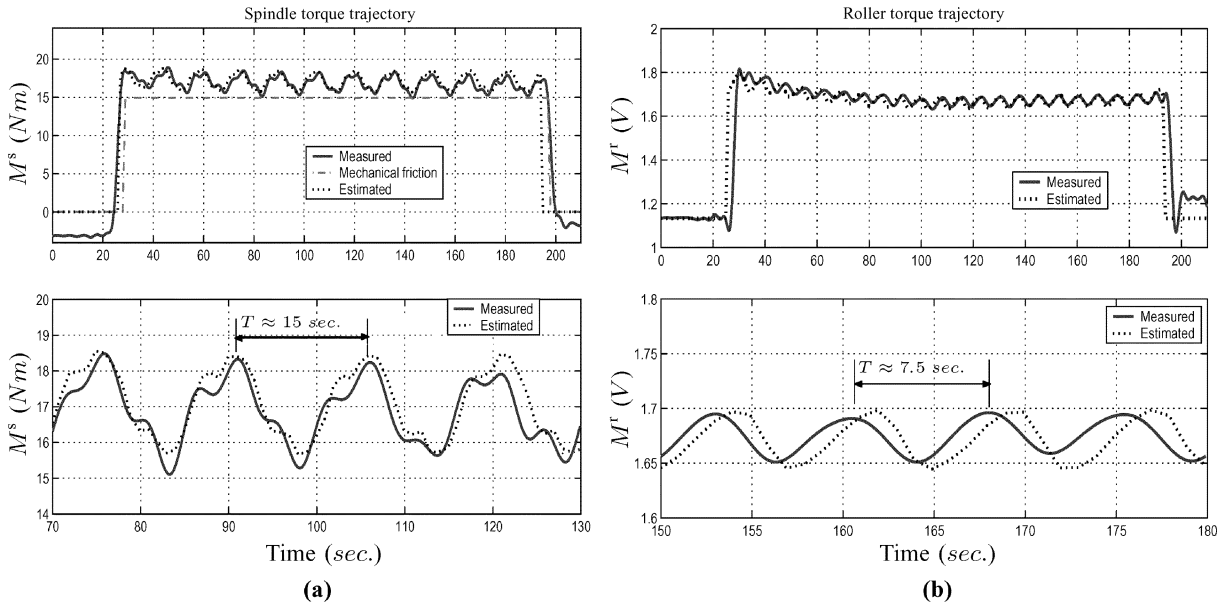

Fig. 7. Example of a baseline process with 100% pad conditioning with conditioner downforce 7 lbf. (a) Spindle motor torque. (b) Roller motor current.

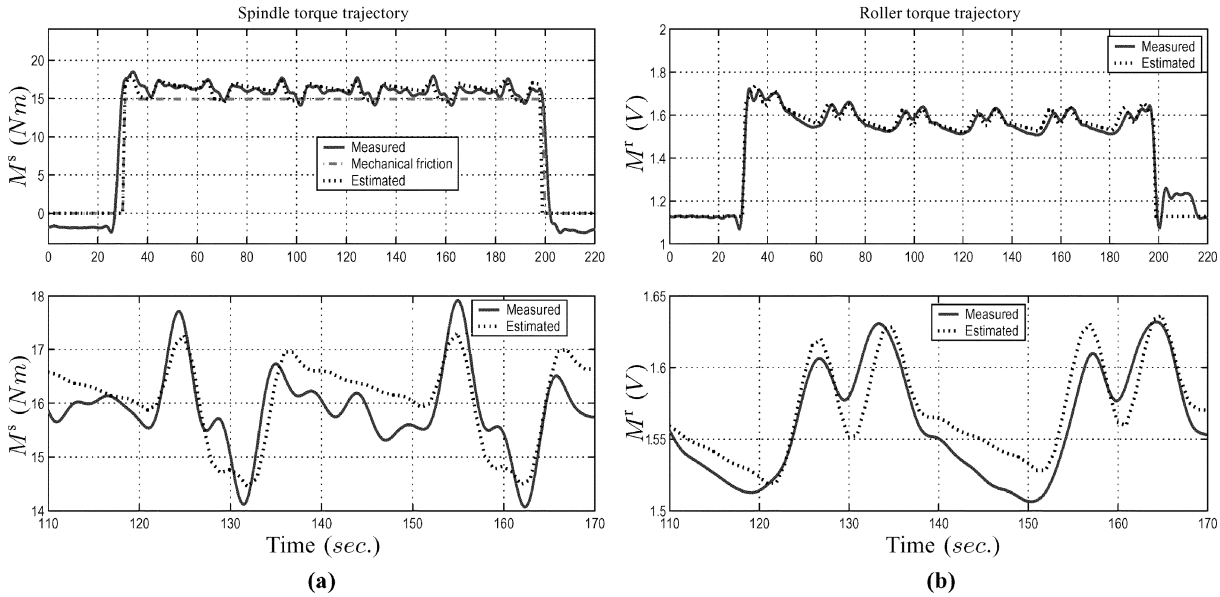

Fig. 8.Example of a baseline process with 50% pad conditioning with a 7 lbf conditioner downforce, (a) Spindle motor torque. (b) Roller motor current.

pad speed (400 ft/min), the spindle torque is close to the mechanical friction torque. The wafer/pad friction moment about the spindle axis is almost zero because the pad speed dominates the relative velocity and the spindle friction torques generated on the front and rear semicircular wafer disks compensate for one another.

The roller motor torque under pad speed variations is quite different from the spindle motor torque. Fig. 11(b) shows the roller motor current change. Considering the decreasing trend due to no pad conditioning, we cannot see any other roller motor torque change during the process except the pad speed transient period. This is consistent with what has been found in [1]: roller motor torque is almost independent of the pad speed [(4)].

3) Wafer Carrier Pressure Variations: A baseline process (pad speed $v_B = 400\ \mathrm{ft/min}$) with varying external wafer carrier pressure is carried out. *Ex situ* pad conditioning and no *in situ* pad conditioning are used in the polishing processes. The process consists of five steps with an 1 psi increase of wafer carrier pressure for each step. Fig. 12 shows the change of the spindle and roller motor torques.

The friction model in [1] implies that both spindle and roller motor torques are proportional to the wafer carrier pressures. From Fig. 12(a), the spindle torque seemingly does not change significantly even though the wafer carrier pressure changes dramatically from 3 to 7 psi (see Fig. 12(c) for a step increase between 30–180 s). This is because the spindle friction moment is small and almost unnoticeable (solid-line minus dot-line in Fig. 12(a) and for most of the time the torque is less than 2 Nm). In contrast, the roller motor torque changes under various wafer carrier pressures are significant [Fig. 12(b)]. Fig. 12(d) shows

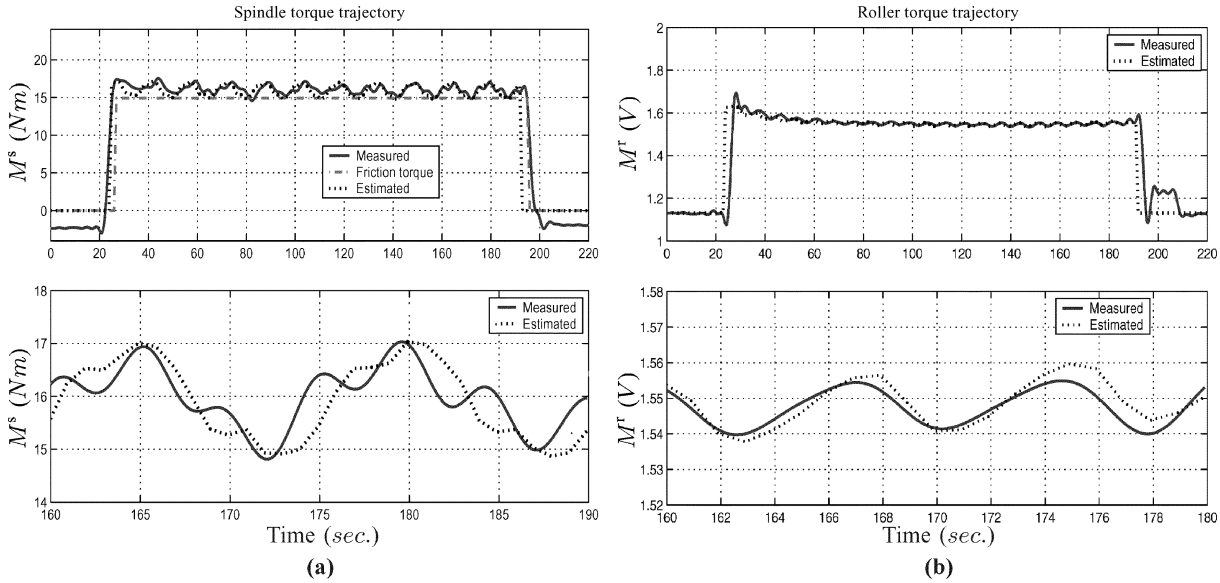

Fig. 9. Example of a baseline process with 100% pad conditioning with a 3 lbf conditioner downforce. (a) Spindle motor torque. (b) Roller motor current.

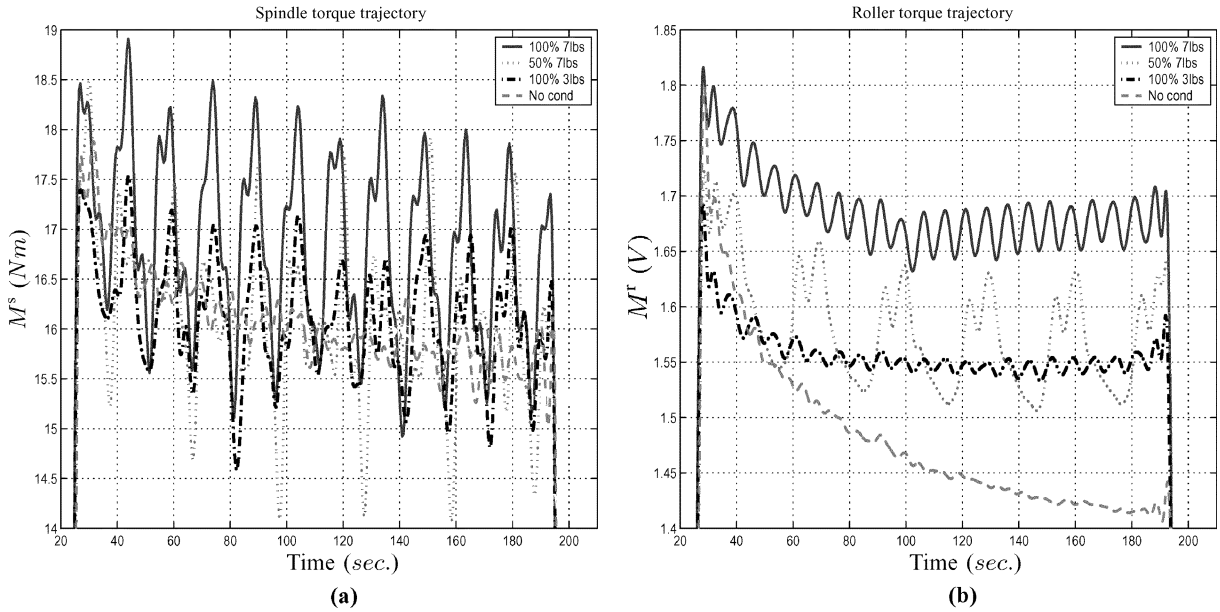

Fig. 10. Comparison of results for various pad conditioning tests. (a) Spindle motor torque. (b) Roller motor current.

the relationship between the roller motor torque value and wafer carrier pressures. There exists a clearly linear relationship (with square of correlation $\mathcal{R}^2 = 0.9769$) between the roller motor torque M^{r} and the wafer carrier pressure p_0.

4) Wafer Carrier Speed Variations: According to the wafer/pad friction model, changing the wafer carrier rotating speed will vary the spindle torque proportionally but has no effect on the roller motor torque. The experimental results in Fig. 13 validate such a fact. There is no direct measurement of carrier rotating speed from the data acquisition system. But we can clearly see the wafer carrier rotating changes from the wafer carrier pressure measurement [Fig. 13(c)]. Since no pad conditioning has been used in the process, roller motor torque does not change but just follows the no pad conditioning decreasing curve [Fig. 13(b)]. For the spindle motor torque [Fig. 13(a)], we can see clearly that it increases when the wafer carrier speed increases. Fig. 13(d) illustrates the relationship between the spindle torque M^{s} and the wafer carrier rotating speed ω. Clearly a linear relationship (with square of correlation $\mathcal{R}^2 = 0.954$) can be observed from the $M^{\mathrm{s}} - \omega$ curve.

V. Applications

In this section, several other examples are described to illustrate the use of spindle and roller motor current measurements to monitor the process performance.

In semiconductor manufacturing production, several dummy wafers (usually 4–8) are used to "warm-up" CMP polishers when the tool is in an idle and "cold" state for a long time. Monitoring the friction level can be used to determine when the

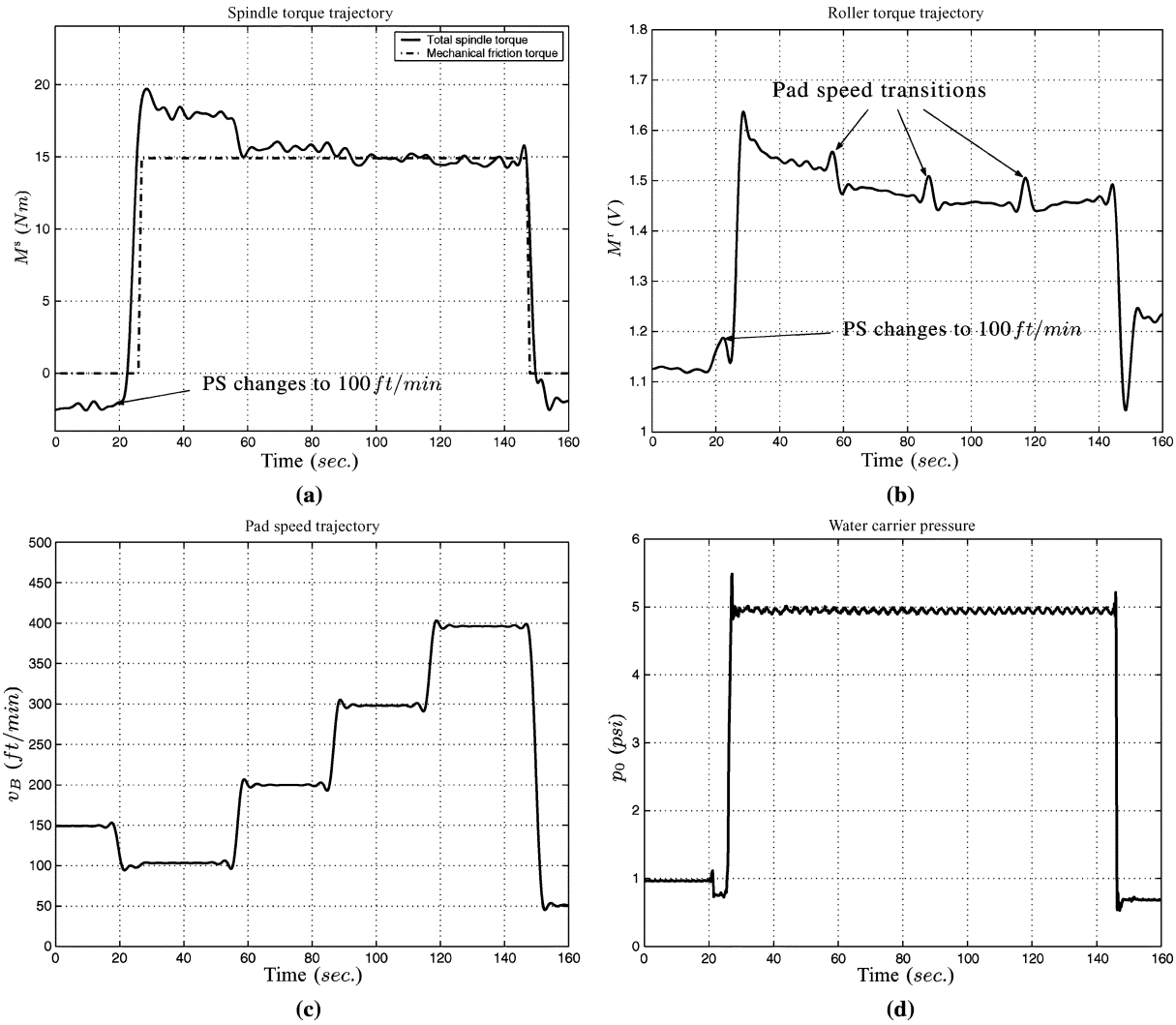

Fig. 11. Torque measurements under different pad speeds. (a) Spindle motor torque. (b) Roller motor current. (c) Pad speed. (d) Wafer carrier pressure.

process is stable. Fig. 14 shows a six-wafer CMP process run when the polisher is coming out of the idle state. The process recipe settings are the same as listed in Table II with a 50% *in situ* pad conditioning (7 lbf conditioner downforce and 7 s per sweep). The process polishing time is 56 s. When the polisher is coming out of the idle state, the polishing pad is cold and there is no slurry distributed on the pad surface. The wafer/pad friction characteristic should be significantly different from the steady-state level. From the spindle motor torque measurements [Fig. 14(a)], we cannot distinguish the differences among the six wafers since the spindle motor torque is relatively small and not sensitive to this difference. The roller motor current measurements, on the other hand, can clearly show the difference between the first and the remaining five wafers. From Fig. 14(b), we can see that roller motor torques for Wafers 2–5 are almost identical and that Wafer 1 is significantly different from the others. The wafer/pad friction coefficient for the first wafer is much higher than the steady-state value since the deformation of the pad asperities is not the same after a long time in the idle state and with rinsing by water. This example demonstrates the use of wafer/pad friction measurements to monitor the run-to-run process variations.

In [1], a pattern factor $\gamma_{\rm patt}$ was defined and used to capture the effect of variations of wafer topography on the wafer/pad friction moments. As an application, we demonstrate one example of friction torque prediction and monitoring when polishing a shallow trench isolation (STI) wafer.[3] Fig. 15 shows the die layout mask of the STI devices that is used for the CMP process testing. Within one die (20 mm $\times$ 20 mm), a set of 25 4 mm $\times$ 4 mm squares are fabricated with various densities and pitches. An SK3 patterned (MIT 961) wafer provided by SKW Associates Inc. is used in the test. The oxide film was deposited by high-density plasma chemical vapor deposition (HDCVD). The average thickness of active oxide across the wafer is 7053 Å and the average trench depth is 7090 Å. The average thickness of the Si_3Ni_4 layer is around 1503 Å. The step height h_{S_0} is around 5000 Å.

Since the density and pitch sizes of each sub-die structure are different, in order to approximately estimate the pattern topography factor $\gamma_{\rm patt}$ for each die, we separate these 25 sub-die structures into two groups: in Group I, the initial step heights are smaller than the contact height, i.e., $h_{S_0} < h_c$ and Group II

[3]For the structure of STI wafers and relevant definitions such as pattern density and pitch width, readers can refer to [1] and [5].

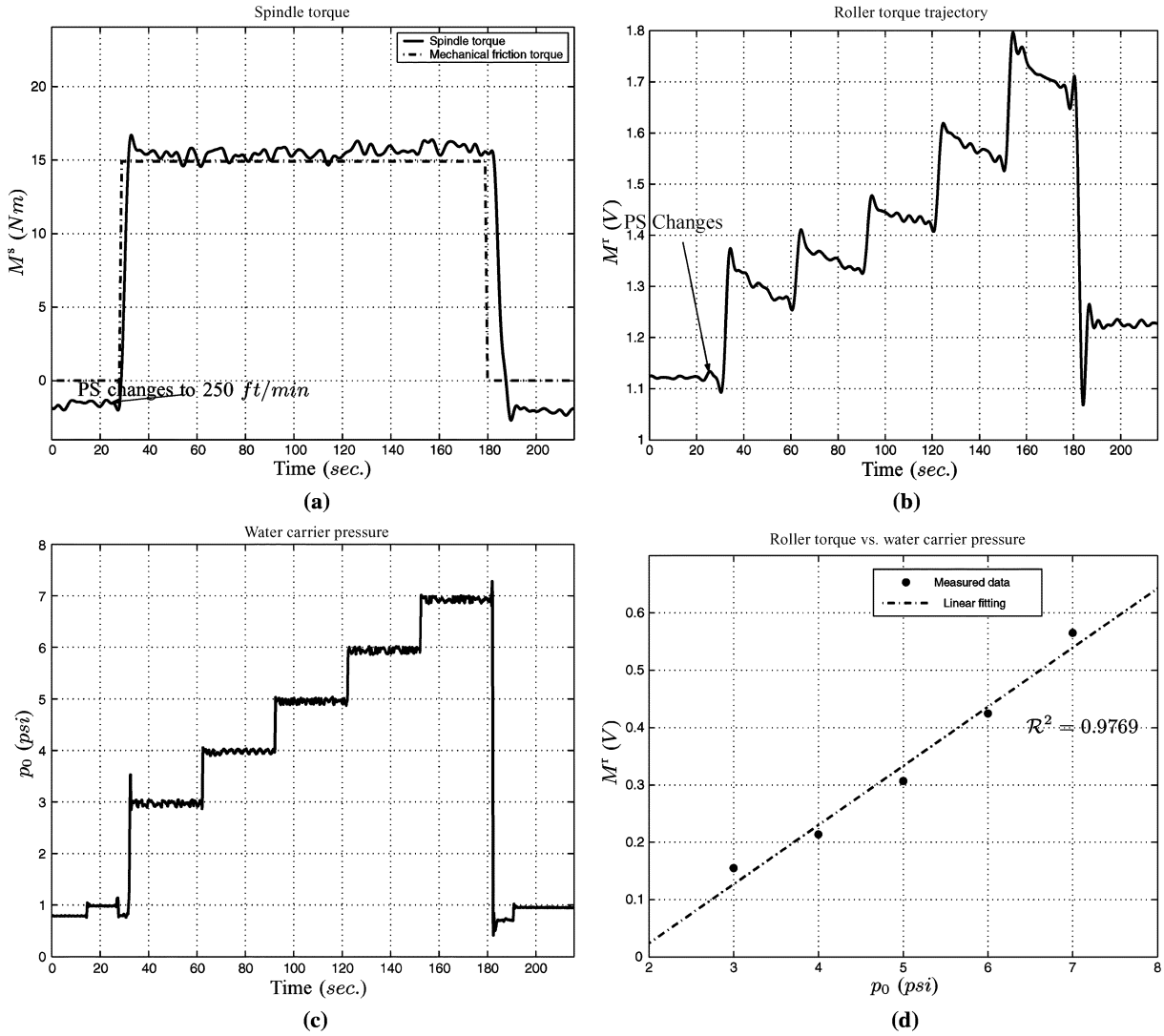

Fig. 12. Torque measurements under various wafer carrier pressures. (a) Spindle motor torque. (b) Roller motor current. (c) Wafer carrier pressure. (d) Roller motor torque versus wafer carrier pressure.

structures have $h_{S_0} \geq h_c$. The analytical results in [1] can be applied to estimate γ_{patt}. For Group I structures that have pitch width $L_0 \geq 100$ μm and pattern density $\rho \geq 50\%$, from [5] an estimate $h_c = 7000$ Å is obtained. For Group II, an estimate $h_c = 4000$ Å is used. From Fig. 15(b), we can calculate the average density for Group I (12 STI structures) $\bar{\rho}_{\text{I}} = 60\%$ and for group II (13 STI structures) $\bar{\rho}_{\text{II}} = 35.4\%$. Then the pattern factors $\gamma_{\text{patt}}^{\text{I}}$ and $\gamma_{\text{patt}}^{\text{II}}$ can be estimated for Groups I and II, respectively. An average factor $\bar{\gamma}_{\text{patt}}$ can be finally calculated as

$$\bar{\gamma}_{\text{patt}} = \frac{n_{\text{I}}\gamma_{\text{patt}}^{\text{I}} + n_{\text{II}}\gamma_{\text{patt}}^{\text{II}}}{n_{\text{I}} + n_{\text{II}}} \tag{17}$$

where n_{I} and n_{II} are the numbers of the STI structures in Groups I and II, respectively. For the mask layout shown in Fig. 15, $n_{\text{I}} = 12$ and $n_{\text{I}} = 13$ and from experimental results in [5] an estimate of $\tau_B = 20$ s is used in the calculation.

Fig. 16 shows the spindle and roller motor torques during the polishing of STI test wafers. The polishing process recipe is the same as the baseline recipe with a longer polishing time (224 s). Torque measurements from polishing an oxide blanket wafer using the same recipe are also plotted in the same figure. Although there is no significant difference in spindle motor torques between the oxide blanket and the STI patterned wafers [Fig. 16(a)], we can clearly notice the difference in the roller motor current measurements [Fig. 16(b)]. When STI patterned wafers are polished, the roller motor current is high for the first few seconds compared with polishing the oxide blanket wafer. This high friction torque is due to the film topography. When the process continues, the wafer surface becomes smooth and the roller motor current follows the blanket oxide polishing trace. After 60 s, the wafer surface becomes planarized. Finally, when the Si_3Ni_4 layer has been polished, the wafer/pad friction increases. The increased wafer/pad friction during the over-polish period could result from two sources: 1) the change of the friction coefficient between the pad and different film layer materials and 2) the dish and erosion effects of the oxide trench areas make the wafer/pad contact pressure increase at the active nitride area.[4] The roller motor current measurement

[4]The estimation of the wafer/pad friction variations during the over-polish period in Fig. 16(b) was calculated by the same approach as shown in [1] and [5].

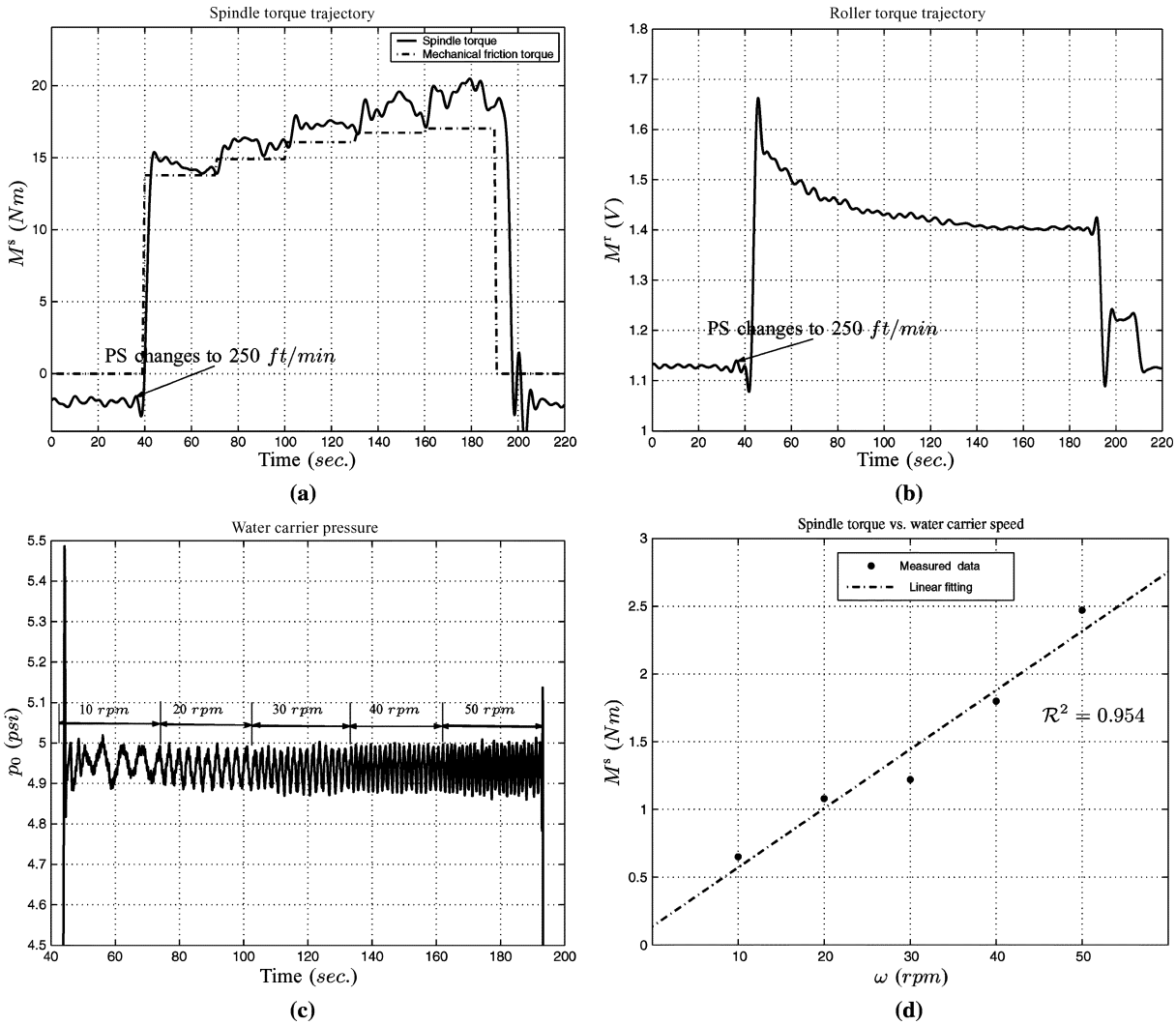

Fig. 13. Torque measurements under various wafer carrier rotating speeds. (a) Spindle motor torque. (b) Roller motor current. (c) Wafer carrier pressure (indicating wafer carrier rotating speed). (d) Spindle motor torque versus the wafer carrier rotating speed.

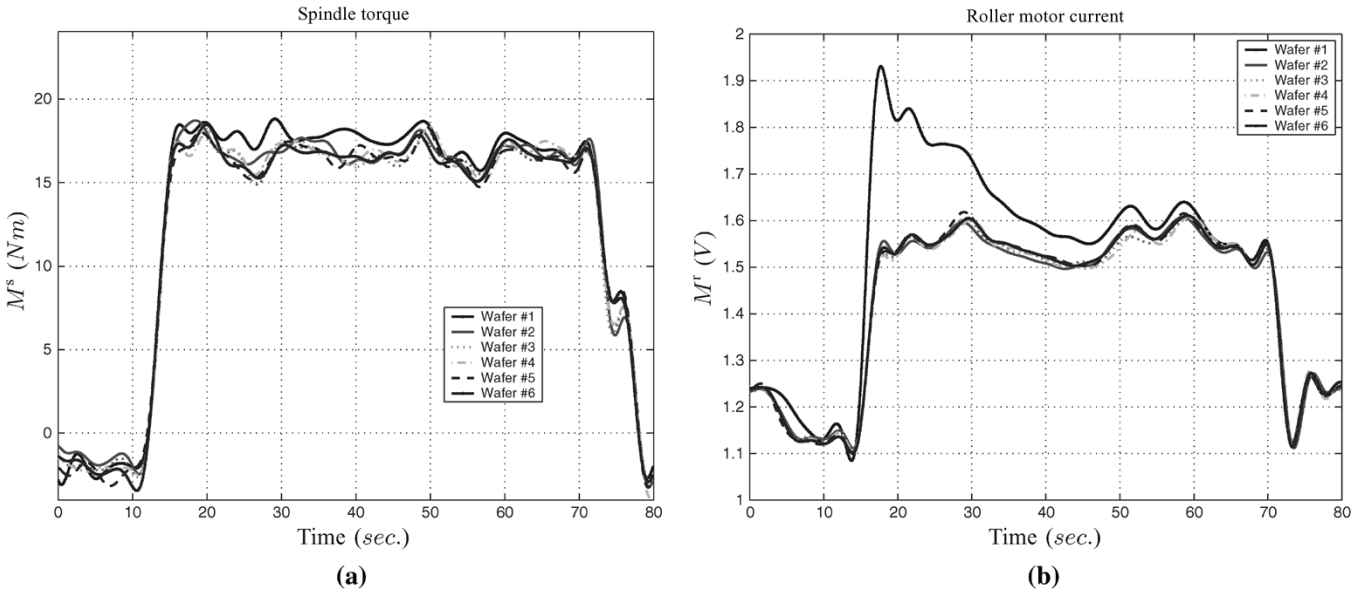

Fig. 14. Friction monitoring for a six-wafer CMP process run coming from the polisher idle state. (a) Spindle motor torque. (b) Roller motor current.

clearly demonstrates the change of the wafer/pad contact and wafer surface planarization.

The estimated roller torque shown in Fig. 16(b) is based on the oxide friction measurement under the same polishing con-

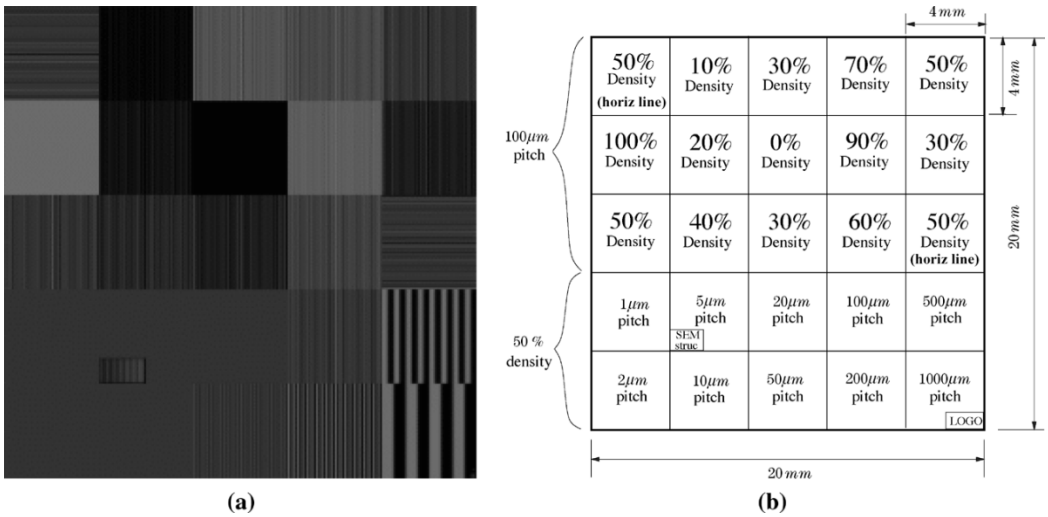

Fig. 15. STI patterned wafer die structure. (a) Layout image. (b) Floor plan and layout mask.

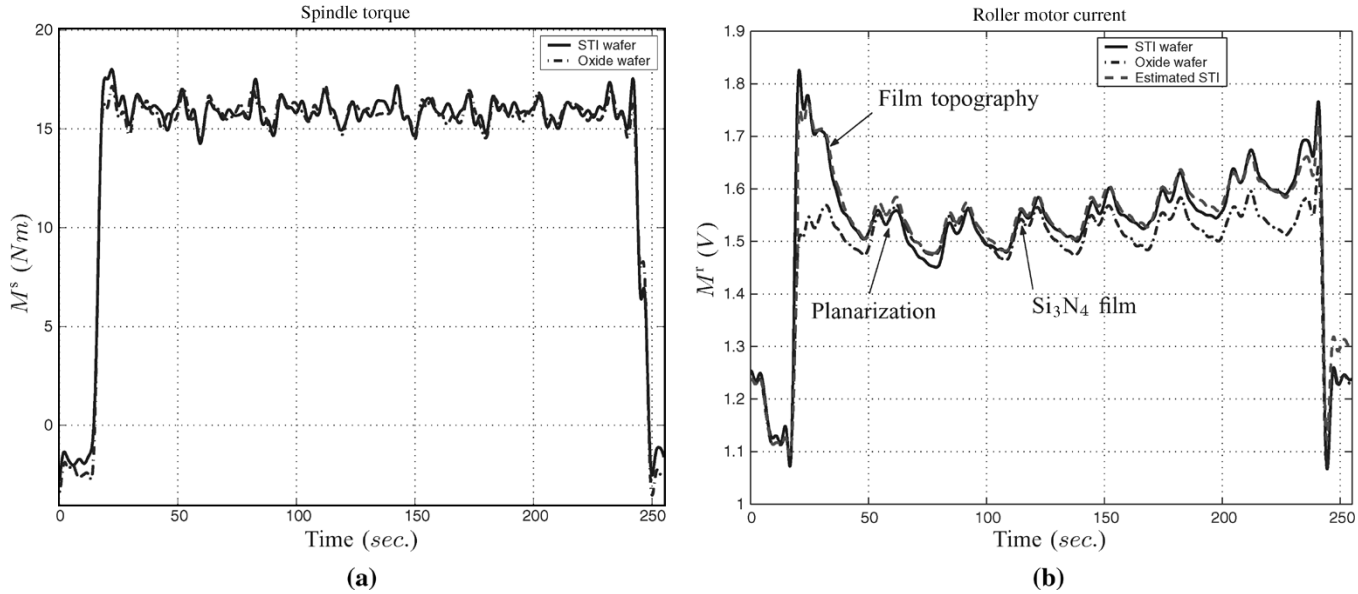

Fig. 16. Measurement comparisons of polishing an STI patterned wafer and an oxide wafer. (a) Spindle motor torque. (b) Roller motor current.

ditions and the pattern effect factor $\bar{\gamma}_{\text{patt}}$. Clearly, it can see a very good fit between the estimated and measured roller torques. Using the estimation of the roller torque, we can monitor the process *in situ*. It is especially useful for CMP processes because of the lack of availability of *in situ* sensors.

Another application example is for the Cu CMP process. Fig. 17 shows the relationship between the dishing average of patterned wafers and the corresponding average roller motor current measurements during a 700-wafer Cu CMP process run. The dishing average is calculated as an average dishing value of a total of 14 dies across the diameter of the 300 mm SEMATECH 754 patterned wafers. Dishing is a critical process specification for a Cu CMP process and it is difficult to obtain such information in real time. The highly linear relationship (with square of correlation $\mathcal{R}^2 = 0.9529$) between the dishing average and roller motor current measurements in Fig. 17 gives the possibility to monitor the dishing performance *in situ*. Using this linear relationship, we can also prepare the consumables and tune the process in real-time to maintain a target dishing level by monitoring the roller motor current measurements.

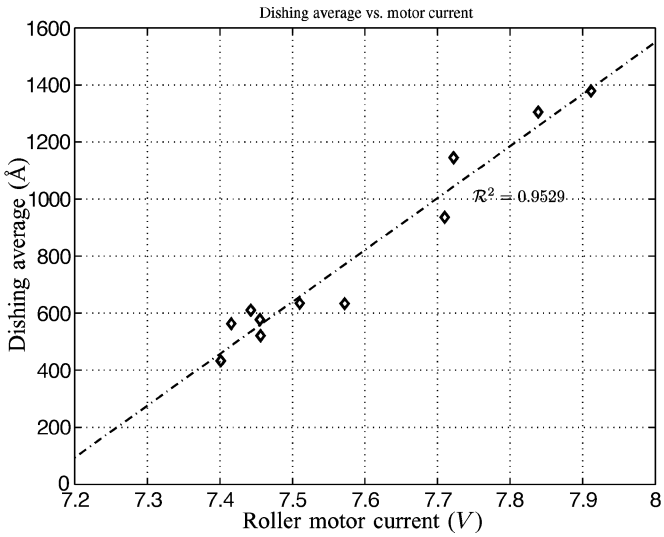

Fig. 17. Relationship of the calculated dishing average and roller motor current measurements for SEMATECH patterned wafers (dash line is the linear fitting curve) during a 700-wafer Cu CMP process run.

VI. Conclusion and Future Work

This paper validated the wafer/pad friction model for a linear CMP process proposed in [1] using a set of comprehensive experiments. Since it is difficult to measure and monitor the wafer/pad friction directly, the polisher's spindle and roller motor current measurements are proposed as the alternative wafer/pad friction indicators. No extra hardware component needs to add to the polisher systems. It has been shown that roller motor torque measurements could be a good candidate to monitor the wafer/pad friction and the polisher systems. The estimations of the spindle and roller motor torques fit the experimental measurements very well. The experimental results have confirmed the theoretical findings and analyzes. Several application examples have been demonstrated to apply the proposed friction modeling and analysis to monitor the CMP processes *in situ*. Although the results in this study are based on linear CMP systems, it is, however, straightforward to extend and apply these methods to other types of CMP platforms, such as orbit and rotary polishers.

The proposed friction modeling and estimation schemes can be further investigated and applied to monitor CMP processes in the future. For example, the proposed schemes can be used as a diagnostic tool for CMP process and polisher systems. Wafer/pad friction produces an energy transformation and the physical temperature will increase on the wafer/pad contact surface. Another future research direction is to use the wafer/pad friction model to investigate how this temperature rise affects the material removal and uniformity mechanisms.

Acknowledgment

The author thanks P. Norton at Lam Research Corporation for his help setting up hardware for data collections.

References

[1] J. Yi, "On the wafer/pad friction of chemical–mechanical planarization (CMP) processes—Part I: Modeling and analysis," *IEEE Trans. Semicond. Manuf.*, vol. 18, no. 3, pp. 359–370, Aug. 2005.

[2] A. K. Sikder, F. Giglio, J. Wood, A. Kumar, and M. Anthony, "Optimization of tribological properties of silicon dioxide during the chemical mechanical planarization process," *J. Electron. Mater.*, vol. 30, no. 12, pp. 1520–1526, 2001.

[3] Y. Homma, K. Fukushima, S. Kondo, and N. Sakuma, "Effects of mechanical parameters on CMP characteristics analyzed by two-dimensional frictional-force measurement," *J. Electrochem. Soc.*, vol. 150, no. 12, pp. G751–G757, 2003.

[4] T. Dyer and J. Schlueter, "Characterizing CMP pad conditioning using diamond abrasives," *MICRO*, Jan. 2002.

[5] B. Lee, "Modeling of chemical mechanical polishing for shallow trench isolation," Ph.D. dissertation, Dept. Elect. Eng. Comp. Sci., Massachusetts Inst. Technol., Cambridge, 2002.

Jingang Yi (S'99–A'02–M'02) was born in Hubei Province, China. He received the B.S. degree in electrical engineering from the Zhejiang University, Hangzhou, China, in 1993, the M.Eng. degree in precision instruments from Tsinghua University, Beijing, China, in 1996, the M.A. degree in applied mathematics, and the Ph.D. degree in mechanical engineering from the University of California, Berkeley, in 2001 and 2002, respectively.

From May 2002 to January 2005, he was with Lam Research Corporation, Fremont, CA, as a Systems Engineer. Since January 2005, he has been with Department of Mechanical Engineering, Texas A&M University, College Station, as a Visiting Assistant Professor. His research interests include intelligent and autonomous systems, mechatronics, automation science, and engineering with applications to semiconductor manufacturing and intelligent transportation systems.

Dr. Yi is the recipient of the Kayamori Best Paper Award of the 2005 IEEE Conference on Robotics and Automation (ICRA).